


Triangulation Sensing to Determine the Gradient Source from Diffusing Particles to Small Cell Receptors

Ulrich Dobramysl^{1,2} and David Holcman³

¹*Department of Applied Mathematics and Theoretical Physics, University of Cambridge, Cambridge CB3 0WA, United Kingdom*

²*Wellcome Trust / CRUK Gurdon Institute, University of Cambridge, Cambridge CB2 1QN, United Kingdom*

³*Group Computational Biology and Data modeling, IBENS, Ecole Normale Supérieure - PSL, Paris, France*

 (Received 11 November 2019; accepted 3 September 2020; published 2 October 2020)

How does a cell locate the source of molecular guidance cues from within a concentration gradient? We present a computational approach to recover the source from the absorbed fluxes at narrow receptor windows located on the surface of the cell. In the limit of fast binding, we solve the steady-state diffusion equation using an asymptotic approach and hybrid stochastic-analytical simulations. We show that the sensitivity to the gradient direction decays too rapidly to enable long-distance sensing. We illustrate how this constraint can be alleviated when triangulating the source with an increasing number of receptor windows and quantify the susceptibility of this process to flux perturbations.

DOI: [10.1103/PhysRevLett.125.148102](https://doi.org/10.1103/PhysRevLett.125.148102)

How do biological cells find a small target site with remarkable precision? This question is ubiquitous in cell biology: spermatozoa need to find the egg in the uterus [1–4]; during brain development, axons migrate toward their final destination by interpreting morphogen gradients via an as of yet unclear mechanisms [Fig. 1(a)] [5–7]. Cells can also decide their migration strategy by combining information from chemical and mechanical gradients that provide guidance to small targets in complex environments [8,9].

The physical principles by which cells find a small target remains poorly understood despite decades of theoretical and experimental works. The first step is the cell ability to detect a local gradient concentration. This question was the subject of Berg and Purcell model, and subsequent significant improvements [10–13]. In their approach, the difference in concentration of diffusing molecules is computed across a small test ball. However, this paradigm is not sufficient to decipher how a cell is able to triangulate the exact position of a gradient source, which goes beyond detecting a gradient concentration [14–16]. Here, the physical model consists instead of many receptors distributed across the surface of a cell that bind diffusing molecules at a fast rate, which differs from [17]. The flux imbalances between different receptors then form a directional signal from which a cell could triangulate the position of the source, thereby identifying its exact location. In a different context, localizing the origin of a disease outbreak (source in a network) requires many spread agents [18].

Triangulating a source in two dimensions requires at least three small receptors to reconstruct the location of the source [15]. However this reconstruction is possible only if the source is exceedingly close—only up to 20 to 40 times the cell diameter. In that case, the level of detection sensitivity decreases with the reciprocal of the distance

to the source. Yet, the axonal growth cone, despite being only a few microns across, nevertheless is able to accurately find its final destination over rather long distances (mm to cm). This paradox was resolved by understanding that migration is constrained to narrow tubes, where triangulation works at much longer ranges due to the asymmetric

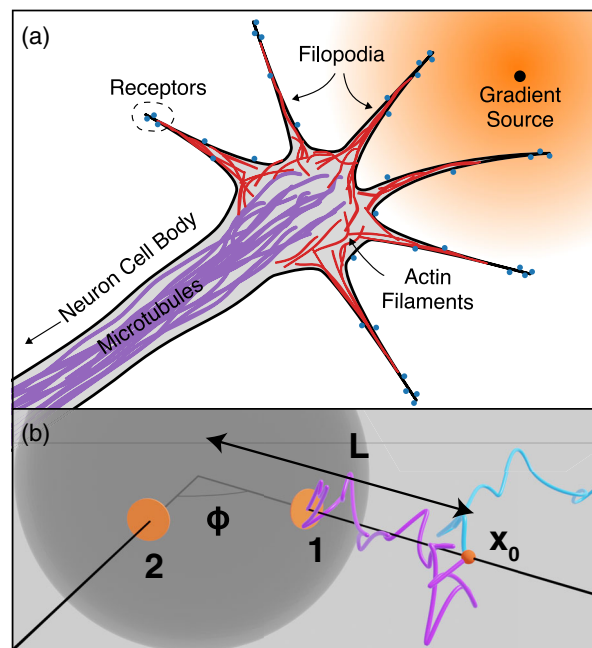


FIG. 1. (a) Neuronal growth cone in an external chemical gradient. Receptors located on the cell surface are able to sense the gradient, thereby defining the first step of navigation in the Brain. (b) Model of sensing: ball containing small windows (receptors). The source is located at x_0 , where Brownian particles are released (blue and purple).

location of the source effectively reducing the search to one dimension [15].

In the present Letter, we study gradient sensing and triangulation in three dimensions using a diffusion model for the molecular cues. We provide an analytical expression for the receptor fluxes using the method of matched asymptotics for the Laplace operator. Using this solution, we determine how the location of the source depends on the position of the receptors. We determine the position of the source for various receptor configurations and show that the sensitivity and susceptibility to noise decay with $1/\sqrt{m}$, where m is the number of receptors.

Diffusion model of cell triangulation.—The model [Fig. 1(b)] consists of diffusing cues that have to bind to M narrow windows located on the surface of three dimensional ball B_a of radius a . Note that in the case of growth cones, a is on the order of $2\text{--}3\ \mu\text{m}$, and M can range between 10 and 50 for, e.g., GABA receptors, but can be much higher for other receptor types. Individual cue molecules are described as Brownian particles. The cues are released from a source at position \mathbf{x}_0 outside the ball [Fig. 2(a)]. Our goal is to estimate the steady-state flux at each narrow window for fast binding (i.e., the probability density has an absorbing boundary condition at the windows). The first step is to solve the Laplace equation

$$D\Delta P_0(\mathbf{x}) = -Q\delta_{\mathbf{x}_0} \quad \text{for } \mathbf{x} \in \mathbb{R}^3 - B_a, \quad (1)$$

where D is the diffusion coefficient in $(\text{cell radii})^2/s$ and Q the number of released particles per unit of time [1/s]. It is always possible to remove these factors by rescaling $P_0 \rightarrow DP_0/Q$. Thus for simplicity we will take D/Q as unity. The boundary conditions are $(\partial P_0/\partial \mathbf{n})(\mathbf{x}) = 0$ for $\mathbf{x} \in \partial B_a - S_k(\varepsilon)$, where $S_k(\varepsilon)$ are nonoverlapping circular windows representing receptors (or possibly clusters thereof) of radius ε centered at points \mathbf{x}_k on the surface of the sphere; the remaining surface of the sphere is absorbing with $P_0(\mathbf{x}) = 0$ for $\mathbf{x} \in \Sigma_a = S_1(\varepsilon) \cup \dots \cup S_m(\varepsilon)$. As \mathbf{x} tends to infinity, the gradient needs to dissipate, hence we use the additional condition $\lim_{|\mathbf{x}| \rightarrow \infty} P_0(\mathbf{x}) = 0$. Using the Green's function approach, a solution of (1) can be found using the Neumann's function [19] for the exterior to a ball in three dimensions

$$\begin{aligned} \mathcal{N}(\mathbf{x}, \mathbf{x}_0) = & \frac{1}{4\pi|\mathbf{x} - \mathbf{x}_0|} + \frac{a}{4\pi|\mathbf{x}_0||\mathbf{x} - \frac{a^2\mathbf{x}_0}{|\mathbf{x}_0|^2}|} \\ & + \frac{1}{4\pi a} \log\left(\frac{|\mathbf{x}_0||\mathbf{x}|}{a^2} [1 - \cos(\theta)]\right), \end{aligned} \quad (2)$$

where $\tilde{d}(\mathbf{x}, \mathbf{x}_0) = 1 - [(\mathbf{x}_0 \cdot \mathbf{x})/a^2] + \{1 + [(\mathbf{x}_0 \cdot \mathbf{x})/a^2]^2 - 2[(\mathbf{x}_0 \cdot \mathbf{x})/a^2]\}^{1/2}$ and $\theta = \angle \mathbf{x}_0 \mathbf{x}$. \mathcal{N} is the solution of the Laplace's equation

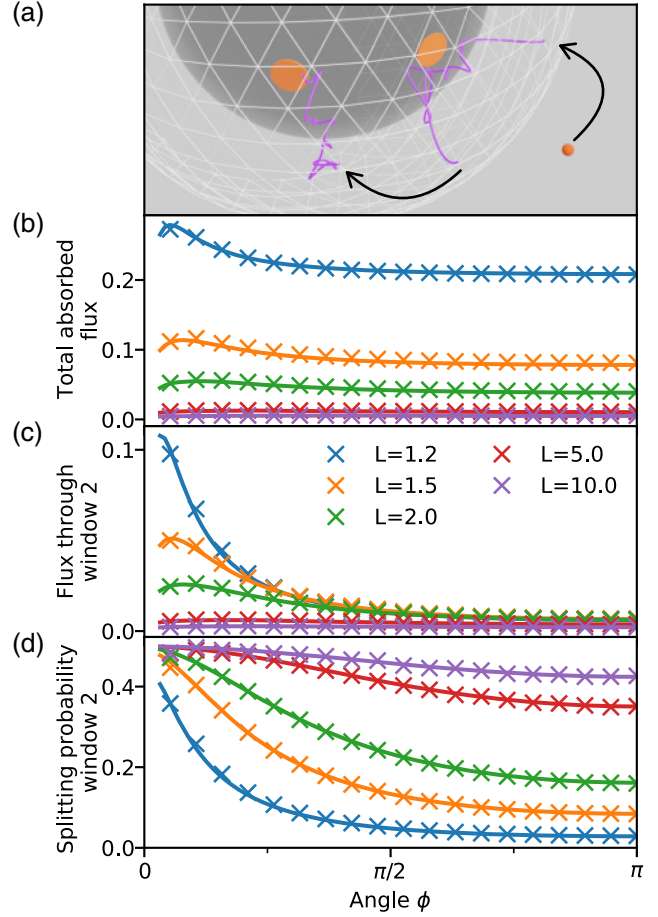


FIG. 2. Diffusion fluxes to two windows. (a) Reflecting ball with window one (orange) facing the source (small orange sphere) and a second window at an angle ϕ . Brownian particles are released by the source (hybrid simulation) either absorbed by one of the windows (magenta) or can escape to infinity. (b) Total flux through both windows vs the angle ϕ , (c) absolute flux through window two, and (d) splitting probability for a particle to hit window two. Curves are for various distance L to the source: analytical results Eq. (6) (solid lines) are compared to simulation data (crosses).

$$\Delta \mathcal{N}(\mathbf{x}, \mathbf{x}_0) = -\delta(\mathbf{x} - \mathbf{x}_0) \quad \text{for } \mathbf{x} \in \mathbb{R}^3, \quad (3)$$

with boundary condition $(\partial \mathcal{N}/\partial \mathbf{n})(\mathbf{x}, \mathbf{x}_0) = 0$ for $\mathbf{x} \in S_a = \partial B_a$, where S_a is the surface of the three-dimensional ball B_a and $\mathbf{x}_0 \in \mathbb{R}^3 - B_a$ the location of the source. Finally,

$$P_0(\mathbf{x}) = \mathcal{N}(\mathbf{x}, \mathbf{x}_0) + \sum_k \int_{\mathbf{y} \in S_k(\varepsilon)} \mathcal{N}(\mathbf{x}, \mathbf{y}) \frac{\partial w(\mathbf{y})}{\partial \mathbf{n}} dS_{\mathbf{y}}. \quad (4)$$

Defining the vector $\tilde{\mathbf{a}}$ with the entries $\alpha_i = -\mathcal{N}(\mathbf{x}_i, \mathbf{x}_0)$, using the unknown fluxes on each window $(\partial P_0/\partial \mathbf{n})(\mathbf{y}) = [A_k/(\sqrt{\varepsilon^2 - r^2})]$, for $\mathbf{y} \in S_k(\varepsilon)$, and Eq. (4), we find that the fluxes follow the matrix equation:

$$[\tilde{\mathbf{M}}]\tilde{\mathbf{A}} = \tilde{\boldsymbol{\alpha}}, \quad (5)$$

where $[\tilde{\mathbf{M}}] = \theta_\varepsilon \mathbf{I} + 2\varepsilon/\pi \mathbf{N}$ and $\theta_\varepsilon = \pi/2 + \varepsilon \log(\varepsilon/a)/(2a) + B\varepsilon$. The constant B (third order in the asymptotic expansion) will be determined numerically. The symmetric matrix \mathbf{N} has zeros on its diagonal and the remaining entries are $[\mathbf{N}]_{ij} = \mathcal{N}(\mathbf{x}_i, \mathbf{x}_j)$ where $i, j = 1, \dots, M$, $i \neq j$. The structure of the matrix $\tilde{\mathbf{M}}$ disallows an explicit solution for any number of windows M , but can be inverted for a fixed M . Finally, after numerically solving Eq. (5), the flux on each window is $\Phi_k = 2\pi A_k$. To first order, the solution is

$$\Phi_k = \theta_\varepsilon^{-1} \left(\alpha_k - \frac{2\pi\varepsilon}{\theta_\varepsilon} \sum_{q \neq k} \mathcal{N}(\mathbf{x}_q, \mathbf{x}_k) \alpha_q \right) + O\left(\left(\frac{2\pi\varepsilon}{\theta_\varepsilon}\right)^2\right). \quad (6)$$

We first confirm the validity of this result using a steady-state hybrid stochastic simulation scheme to compute these fluxes: briefly, after Brownian particles are released from the source $S(\mathbf{x}_0)$, their position is immediately mapped to a test surface which consists of a sphere ∂B_R around the ball B_a , with $R \gg a + \varepsilon$ [Fig. 2(a)]. The distribution of mapped points is given by the mapping

$$P(\mathbf{x}; \mathbf{x}_0) = \frac{1}{4\pi} \frac{\beta^2 - 1}{(1 + \beta^2 - 2\beta \cos \gamma)^{3/2}}, \quad (7)$$

which represents the flux through the absorbing boundary ∂B_R in free space, here $|\mathbf{x}| = R$, $|\mathbf{x}||\mathbf{x}_0| \cos \gamma = \mathbf{x} \cdot \mathbf{x}_0$ and $\beta = |\mathbf{x}_0|/R$. After mapping to the initial position, a particle performs a Brownian motion (Euler-Maruyama scheme) until it is absorbed by a window. A particle can also leave the test ball of radius $R_e > R$ (this larger radius exists to prevent frequent mappings), upon which it is mapped back to the surface ∂B_R using Eq. (7). For each mapping, a particle has a finite probability $P_e = R/|\mathbf{x}_0|$ to escape to infinity, whereupon its trajectory is terminated.

Accuracy in recovering the direction of a source only.—To illustrate the insight of the model, we start with two windows located on the equator of the ball [Fig. 2(a)]: window one faces the source directly and window two is at an angle ϕ . The total flux through both windows vs the source distance $L = |\mathbf{x}_0|$ and the angle ϕ shows excellent agreement [Fig. 2(b)] between the analytical results (solid lines) and simulated data (crosses), with the single fit parameter $B = 5.7$. The flux through window two alone [Fig. 2(c)] shows a single maximum when the windows are close and decays rapidly to a small but finite value when the window is on the opposite side of the ball. The splitting probability $p_S = [\Phi_1/(\Phi_1 + \Phi_2)]$ of hitting window two given that a particle hits one of the windows allows for distinguishing the direction only of the source when it is very close. Already for $L = 10$ ball radii, the difference in the hitting probabilities is smaller than 10%, which

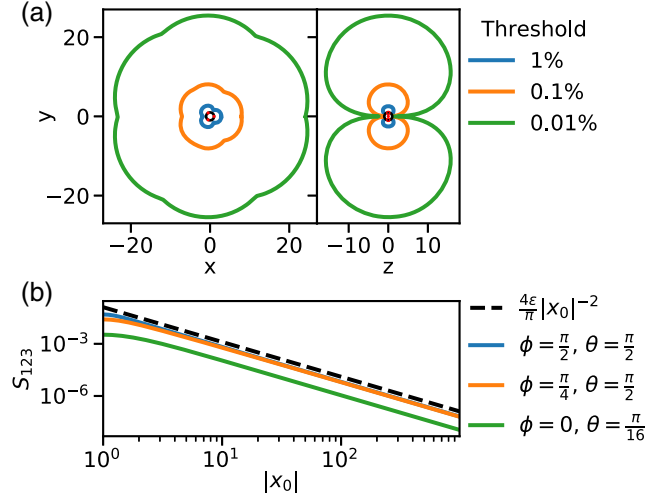


FIG. 3. Sensitivity of detecting the source position from Eq. (8). (a) A ball with three windows arranged as an equilateral triangle. The detection contours is in the plane that contains all three windows (left) and in plane perpendicular to the window plane (right), for three different detection thresholds (1%, 0.1%, and 0.01%). (b) The sensitivity decays with $1/|\mathbf{x}_0|^2$ for the source position \mathbf{x}_0 . Distances are measured in units of the cell radius.

illustrates the difficulty of direction sensing over long distances.

To quantify the distance at which it is still possible to recover the direction of the source with three windows, we use the sensitivity cost function

$$S_{123}(\mathbf{x}_0) = \max\{|P_1(\mathbf{x}_0) - P_2(\mathbf{x}_0)|, |P_2(\mathbf{x}_0) - P_3(\mathbf{x}_0)|, |P_3(\mathbf{x}_0) - P_1(\mathbf{x}_0)|\}, \quad (8)$$

where \mathbf{x}_0 is the position of the source and \mathbf{x}_i , $i = 1, 2, 3$ are the positions of the three windows on ∂B_a . The cost function $f(\mathbf{x}_0; \mathbf{x}_1, \mathbf{x}_2, \mathbf{x}_3)$ describes the maximum absolute imbalance between the fluxes through the windows. Figure 3(a) shows the contours of this function for three windows arranged in an equatorial equilateral triangle in a slice through the $z = 0$ and $\mathbf{x} = 0$ planes at three different threshold levels. Notably, the distance at which directions can still be discerned is approximately an order of magnitude less for any given threshold compared to the equivalent situation in two dimensions [15]. Indeed, using the dipole expansion for a source located far away $|\mathbf{x}_0| \gg 1$, $f(\mathbf{x}_0; \mathbf{x}_1, \mathbf{x}_2, \mathbf{x}_3) \approx [C/(|\mathbf{x}_0|^2)]$ where $C > 0$ is constant. Figure 3(b) illustrates this decay.

Triangulating the source location.—To reconstruct the location of a source \mathbf{x}_0 (three coordinates of the source) from the measured fluxes Φ_i received at windows located at position \mathbf{x}_i , we require at least three windows. Interestingly, in two dimensions the minimum number of windows is three as well, even though only two coordinates need to be determined. The source location \mathbf{x}_0 enters Eq. (5) only via the Neumann-Green's function \mathcal{N} , which we invert

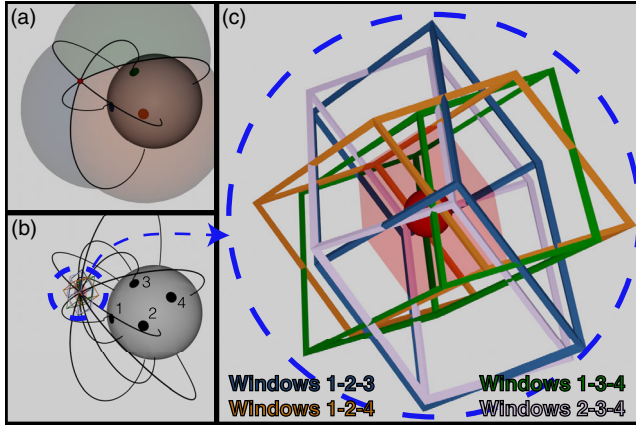


FIG. 4. Triangulation of the source position with three out of four windows. (a) Triangulation using three fluxes F_1, F_2, F_3 . (b) Four windows yield redundant intersection lines. (c) Enlargement of the area around the source in (b). Each combination of three windows defines a volume around the source position (here for a fixed perturbation $\eta = 0.001$ of the fluxes), computed from combining three out of four windows (colors).

numerical by rewriting Eq. (5) as a solution of the implicit equations

$$F_i(\mathbf{x}_0) = \theta_\epsilon \Phi_i + \sum_{j \neq i} \mathcal{N}(\mathbf{x}_i, \mathbf{x}_j) \Phi_j - 2\pi \mathcal{N}(\mathbf{x}_i, \mathbf{x}_0) = 0.$$

Each of the m equations describes a closed surface in three dimensions, the intersection of which yields the source location. Therefore, we use the following procedure: we search for the joint root of the $F_i(\mathbf{x}_0)$ by tracing the root contour of F_1 in the x - y plane until we find its intersection with the root contour of F_2 . We then plot the curve described by the joint root contour of F_1 and F_2 until $F_3 = 0$ is fulfilled [Fig. 4(a)]. This yields the source location \mathbf{x}_0 as a function of the measured fluxes F_i and the window locations \mathbf{x}_i . The choice of window labels used in this algorithm is arbitrary and we could have used any combination of three of the m windows.

Susceptibility of the reconstruction to flux noise.—In order to estimate the susceptibility of the triangulation to small perturbations, we define the noisy flux coordinates $\tilde{\Phi}_i = K_i/N_t$, where $i = 1, \dots, m$ and $K_i \sim \text{Multi}(N_t, \{\Phi_1, \dots, \Phi_m, 1 - \sum_{i=1}^m \Phi_i\})$ are multinomially distributed with $N_t = 10^7$ trials (the smaller N_t the noisier the resulting fluxes). For each combination of three windows j, k, l out of $n = m(m-1)(m-2)/6$, we calculate the recovered position $\tilde{\mathbf{x}}^r$, $r = (j, k, l)$, using the procedure described above. These positions will all be shifted relative to each other due to the stochastic perturbation, hence the final estimator of the source position is $\hat{\mathbf{x}}_m = \sum_{r=1}^n \mathbf{x}_r/n$ where $n = m(m-1)(m-2)/6$ the number of combinations. To measure the susceptibility to random fluxes, we plot the radius $R_{99}(m, L)$ around \mathbf{x}_0 in which 99% of recovered

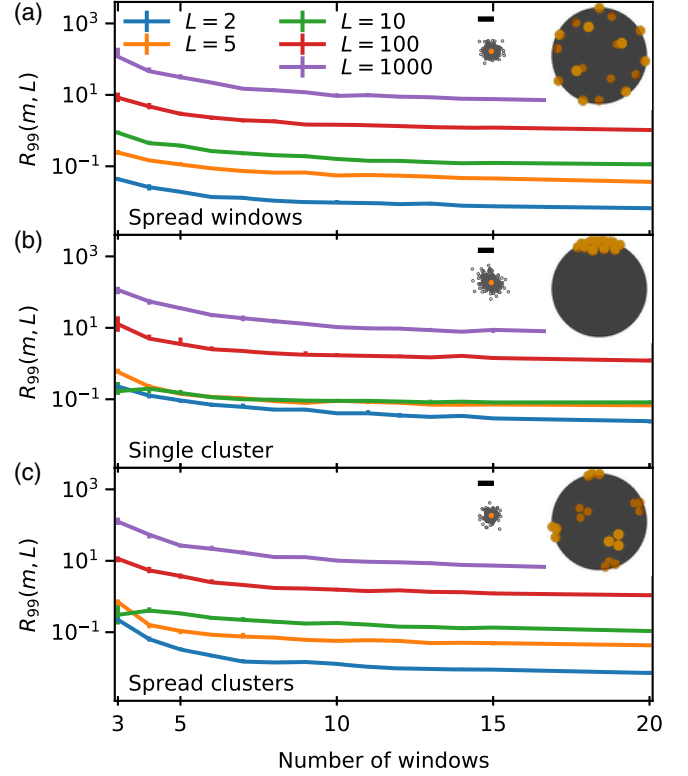


FIG. 5. Uncertainty of the source location. Deviation of the reconstructed source from its exact position measured by the radius R_{99} around \mathbf{x}_0 in which 99% of recovered points fall, when the fluxes are subject to multinomial noise with $N_t = 10^7$ trials. The source location is computed by averaging over reconstructions from all combinations of three windows. R_{99} is calculated from 1000 realizations and random source positions (with $|\mathbf{x}_0| = L$ fixed). (a) Windows are spread uniformly across the ball surface, (b) a single cluster of windows, and (c) window clusters are spread uniformly across the ball surface (at most three windows per cluster). The error bars indicate the 95% confidence interval. The insets show the spread of points around the exact source position for $L = 5$ and $m = 5$ (scale bar corresponds to one-tenth of the ball radius).

points fall out of 1000 independent realizations of the $\tilde{\Phi}_i$ (Fig. 5). We examine three window configurations (with the exact source randomly located on a shell with radius L): spread uniformly across the ball surface [Fig. 5(a)], concentrated in a single cluster [Fig. 5(b)], and window clusters spread uniformly across the surface [Fig. 5(c)]; see the Supplemental Material [20] on the window position algorithm. Stochastic simulations show a reduction in R_{99} with an increasing number of windows in all cases [Fig. 5(a)]. For $m \geq 9$, R_{99} scales roughly as $m^{-1/2}$ (Fig. S2). Case A shows a better accuracy for small L and low m than cases B and C [Figs. 5(a)–5(c)]. The dip in R_{99} for small m in cases B and C [Figs. 5(b), 5(c) and S1(b), S1(c)] is driven by a thinning of the angular spread of the recovered points at certain orientations [Figs. S3(b), S3(c) and S4]. At large m , all three cases converge to similar accuracy. We can also

compute the positional uncertainty by using a Taylor expansion $\tilde{\mathbf{x}}^r(\tilde{\Phi}_j, \tilde{\Phi}_k, \tilde{\Phi}_l) = \mathbf{x}_0 + J_r \boldsymbol{\eta} + O(\sigma^2)$, where J_r is the Jacobian of \mathbf{x}_0 with respect to the fluxes and $\boldsymbol{\eta} = (\eta_j, \eta_k, \eta_l)$. The deviation can then be estimated by $\sqrt{\langle |\mathbf{x}_0 - \hat{\mathbf{x}}_m|^2 \rangle} \sim (\sigma/\sqrt{m})$ [20].

Concluding remarks.—Because the arrival of Brownian particles to small windows is Poissonian, the particle fluxes to receptors on the cell surface can be measured in finite time empirically by a counting process. Detection of the direction of an external gradient in three dimensions with only three windows is only possible at exceedingly short distances compared to the two-dimensional case (especially when the cell is placed in a corridor) [15]. Here we showed that triangulation of the source position and the precision that increase with the number of receptors, can counter this decay in directional sensitivity. This can allow in principle the recovery of a gradient source positions at large distances. The framework we developed is especially suited to slow-growing cell projections, such as neuronal growth cones [5] that have to identify their spatial location in a gradient field and to ultimately migrate to a final destination. Future work needs to address how cells integrate the external cue signals and also deal with multiple gradient sources to make navigation decisions [21,22].

A similar question generalizing Ref. [15] in three dimensions was addressed in Lawley *et al.* [23] during the review process of this manuscript.

U. D. gratefully acknowledges support through a Herchel Smith Postdoctoral Fellowship. D. H is supported by an ANR NEUC-0001

-
- [1] B. M. Friedrich and F. Jülicher, *Proc. Natl. Acad. Sci. U.S.A.* **104**, 13256 (2007).
 - [2] U. B. Kaupp and T. Strünker, *Trends Cell Biol.* **27**, 101 (2017).
 - [3] T. Strünker, L. Alvarez, and U. Kaupp, *Curr. Opin. Neurobiol.* **34**, 110 (2015).

- [4] L. Alvarez, B. M. Friedrich, G. Gompper, and U. B. Kaupp, *Trends Cell Biol.* **24**, 198 (2014).
- [5] A. Chédotal and L. J. Richards, *Cold Spring Harbor Perspect. Biol.* **2010**, a001917 (2010).
- [6] G. J. Goodhill, *Trends Neurosci.* **39**, 202 (2016).
- [7] J. Reingruber and D. Holcman, in *Seminars in Cell & Developmental Biology* (Elsevier, New York, 2014), Vol. 35, pp. 189–202.
- [8] M. Gorelashvili, M. Emmert, K. F. Hodeck, and D. Heinrich, *New J. Phys.* **16**, 075012 (2014).
- [9] J. A. Wondergem, M. Mytiliniou, F. C. de Wit, T. G. Reuvers, D. Holcman, and D. Heinrich, *bioRxiv* 735779 (2019).
- [10] H. C. Berg and M. Purcell, *Biophys. J.* **20**, 193 (1977).
- [11] R. Zwanzig, *Proc. Natl. Acad. Sci. U.S.A.* **87**, 5856 (1990).
- [12] R. G. Endres and N. S. Wingreen, *Proc. Natl. Acad. Sci. U.S.A.* **105**, 15749 (2008).
- [13] K. Kaizu, W. De Ronde, J. Pajmans, K. Takahashi, F. Tostevin, and P. R. Ten Wolde, *Biophys. J.* **106**, 976 (2014).
- [14] U. Dobramysl and D. Holcman, *J. Comput. Phys.* **355**, 22 (2018).
- [15] U. Dobramysl and D. Holcman, *Sci. Rep.* **8**, 941 (2018).
- [16] O. Shukron, U. Dobramysl, and D. Holcman, *Chemical Reactions for Molecular and Cell Biology*, edited by K. Lindenberg, R. Metzler, and G. Oshanin, Chemical Kinetics Beyond the Textbook (World Scientific Europe, 2019).
- [17] H. C. Berg, *Random Walks in Biology* (Princeton University Press, Princeton, 2018).
- [18] P. C. Pinto, P. Thiran, and M. Vetterli, *Phys. Rev. Lett.* **109**, 068702 (2012).
- [19] T. Lagache and D. Holcman, *J. Stat. Phys.* **166**, 244 (2017).
- [20] See the Supplemental Material at <http://link.aps.org/supplemental/10.1103/PhysRevLett.125.148102> for the dependence of the susceptibility on the receptor number, organization and distance to the source.
- [21] C. Bouzigues, M. Morel, A. Triller, and M. Dahan, *Proc. Natl. Acad. Sci. U.S.A.* **104**, 11251 (2007).
- [22] C. Bouzigues, D. Holcman, and M. Dahan, *PLoS One* **5**, e9243 (2010).
- [23] S. D. Lawley, A. E. Lindsay, and C. E. Miles *Phys. Rev. Lett.* **125**, 018102 (2020)